Eur. Phys. J. A **18**, 87–92 (2003)
DOI 10.1140/epja/i2003-10063-9

THE EUROPEAN PHYSICAL JOURNAL A

Multiple Coulomb excitation experiment of ^{66}Zn

M. Koizumi[1,a], A. Seki[1,2], Y. Toh[1], M. Oshima[1], A. Osa[1], A. Kimura[1], Y. Hatsukawa[1], T. Shizuma[1], T. Hayakawa[1], M. Matsuda[1], J. Katakura[1], T. Czosnyka[3], M. Sugawara[4], T. Morikawa[5], and H. Kusakari[6]

[1] Japan Atomic Energy Research Institute, Tokai, Ibaraki 319-1195, Japan
[2] Graduate School of Science & Engineering, Ibaraki University, Bunkyo 2-1-1, Mito, Ibaraki 310-8512, Japan
[3] Heavy Ion Laboratory, Warsaw University, Pasteura 5a, 02-093 Warszawa, Poland
[4] Chiba Institute of Technology, Narashino, Chiba 275-0023, Japan
[5] Kyushu University, Hakozaki, Fukuoka 812-8581, Japan
[6] Chiba University, Inage-ku, Chiba 263-8522, Japan

Received: 28 January 2003 / Revised version: 18 March 2003 /
Published online: 9 October 2003 –
Communicated by D. Schwalm

Abstract. A Coulomb excitation experiment was carried out with a ^{66}Zn beam bombarding a ^{nat}Pb target. Four $E2$ matrix elements and the quadrupole moment of the 2_1^+ state were derived with the least-squares search code GOSIA. According to the $B(E2)$ values, the ground band can be interpreted as a quasirotational band. It was found that the 2_1^+ level has a positive quadrupole moment, which may be interpreted as a soft triaxial deformation.

PACS. 25.70.De Coulomb excitation – 21.10.Ky Electromagnetic moments – 23.20.-g Electromagnetic transitions – 27.50.+e $59 \leq A \leq 89$

1 Introduction

Having two extra protons outside the $Z = 28$ closed shell, stable even-even Zn nuclei are generally interpreted with collective vibrational models, which show the familiar pattern with the 2_1^+ state and the triplet of 0_2^+, 2_2^+, and 4_1^+ states at about twice the energy of the 2_1^+ state. Nevertheless, the Zn isotopes cannot be treated as typical vibrational nuclei. For ^{64}Zn and ^{66}Zn, an enhancement of the $E2$ transition probabilities was found between the states in the ground band, and between the states in the excited band based on the 2_2^+ state, while those of the inter-band transitions are weak [1–4]. The low-lying states of those nuclei can be, therefore, interpreted as quasirotational bands. The behavior of the 0_2^+ of Zn isotopes is also interesting; the excitation energy of the 0_2^+ states decreases as the neutron number increases until $N = 40$. This 0_2^+ state's behavior may be explained with the influence of the $1g_{9/2}$ orbit, because simple shell model calculation carried out by Hienen *et al.* [5], in which the $1g_{9/2}$ orbit was neglected, reproduced generally well the states except for the 0_2^+. Near the Zn isotopes, shape coexistences were found in Ge and Se isotopes [6–9]. Large triaxial deformations in the ground states of $^{72-76}$Ge and $^{74-78}$Se were pointed out in refs. [10,11]. These nuclei are located in the same transitional region between $N = 28$ and 40, where various non-spherical shell gaps exist in a Nilsson diagram. Thus, the experimental interests here are in the $B(E2)$ values and quadrupole moments of Zn isotopes.

The pattern of the low-lying energy levels of ^{66}Zn seems to be a characteristic of vibrational nuclei at first glance as mentioned above. Specifically, the excitation energy ratios $E(I)/E(2_1^+)$ of the 0^+, 2^+, and 4^+ states are about two. The ratios of $B(E2)$ values are $B(E2; 4_1^+ \rightarrow 2_1^+)/B(E2; 2_1^+ \rightarrow 0_1^+) \sim 2.0$ [12], which can be interpreted as a vibrational pattern, too. The ratio $B(E2; 2_2^+ \rightarrow 2_1^+)/B(E2; 2_1^+ \rightarrow 0_1^+) \sim 20$ [12] is, however, too large. The transition probability $B(E2; 2_2^+ \rightarrow 2_1^+)$ is extraordinarily enhanced. As for the other Zn isotopes, no such enhanced $2_2^+ \rightarrow 2_1^+$ transition was observed. In reviewing the $B(E2)$ values of ^{66}Zn, most of them were deduced from lifetime measurements, and their experimental values except for the $B(E2; 2_1^+ \rightarrow 0_1^+)$ are too scarce to determine the reliable values; for example, the experimental lifetimes of the 2_2^+ state were $1.0^{+0.8}_{-0.2}$ ps [13], $1.2^{+0.5}_{-0.3}$ ps [14], 0.27 ± 0.10 ps [15], and $1.1^{+0.6}_{-0.3}$ ps [16]. Therefore, it would be important to experimentally confirm these $B(E2)$ values for understanding the low-lying structure of ^{66}Zn.

Multiple Coulomb excitation of projectile nuclei with a heavy target enables us to populate excited states up to about 2 MeV. With this technique, quadrupole moments

[a] e-mail: koizumi@jball4.tokai.jaeri.go.jp

and $B(E2)$ transition probabilities of low-lying levels can be derived model independently [17–19]. In the Tokai site of Japan Atomic Energy Research Institute (JAERI), we have developed an apparatus for Coulomb excitation experiments and installed it at the tandem and booster accelerator facility, which can provide heavy-ion beams with an energy of the Coulomb barrier for the heavy targets [20, 21]. In this study, we carried out a Coulomb excitation experiment of ^{66}Zn, and analyzed the experimental data with the least-squares search code GOSIA [22,23]. The $B(E2)$ values were revised, and the quadrupole moment of the 2_1^+ state was newly determined.

2 Experiment

Multiple Coulomb excitation experiment of ^{66}Zn was carried out at the tandem and booster accelerator facility of Tokai/JAERI with a 274.2 MeV ^{66}Zn beam bombarding a self-supporting $^{\rm nat}$Pb target with a thickness of 1.7 mg/cm^2. De-excitation γ-rays from the excited nuclei were measured with a γ-ray detector array, GEMINI [20], and scattered incident particles were detected with a position-sensitive particle detector array, LUNA [21].

The GEMINI consisted of 12 HPGe detectors with BGO anti-Compton suppressors, which were arranged spherically at a distance of 13 cm from the target. A lead collimator was mounted in front of each detector in order to reduce the effect of Doppler shift. This resulted in reducing the geometrical solid angle to be 0.6% of 4π. The relative detection efficiency of each Ge detector was 40–70% with respect to a $3'' \times 3''$ NaI scintillator. The energy resolution of the Ge detectors was about 2.2 keV FWHM for the 1.3 MeV γ-rays from a ^{60}Co source.

The position-sensitive particle detector array consisted of four position-sensitive photomultiplier tubes covered with a scintillator plate [21], the sensitive area of which was 22 mm square. It covered about 30% of total solid angle. The positional resolution was 1.2 mm FWHM near the edge of the detector and 0.5 mm FWHM near the center; they correspond to the angular resolution of 3.7° and 1.9° FWHM, respectively.

The output signals from the Ge and particle detectors were processed by standard NIM/CAMAC modules, and sent to a data acquisition system controlled by a real-time Linux computer on a VME bus. The system acquired event-by-event data of particle-γ coincidence consisting of the γ-ray energy, the pulse heights of the signals from the position-sensitive particle detector outputs [21], and the time difference between the particle and γ-ray signal. The acquired data were transferred to a FreeBSD-based computer and stored on digital data storage (DDS) tapes. After about 65 h bombardment with an average beam current of about 5 nA, we obtained about 1.5×10^8 events.

3 Analysis and results

The Doppler shift of γ-ray energy was corrected event by event using the angle between the γ-ray and the scattered particle. Figure 1 shows one of the spectra obtained after the Doppler correction, in which three transitions are clearly seen. In this analysis, the position-sensitive particle detectors in each side of the beam were divided into seven segments along the scattering angle; the forward detectors were divided into four and the backward detectors into three. The mean scattering angle of each segment represents the impact parameter of the Rutherford scattering; the individual scattering angles were 34.5°, 43.8°, 52.0°, 61.4°, 120.2°, 134.5°, and 151.9°. Then, a data set of γ-yields for each Ge detector in coincidence with each particle segment was prepared. In addition, the spectroscopic data and their errors given in table 1 were also added to the data set. The values of experimental lifetimes of the 2_2^+ and 4_1^+ were omitted because they are too scarce to determine a reliable value as mentioned above. For the $E2/M1$ mixing ratio, there exist three measurements, which are -2.6 ± 0.3 [16], -1.9 ± 0.3 [24], and -2.3 ± 0.7 [25]. These values did not change the results except for $\langle 2_1^+ || M1 || 2_2^+ \rangle$, and the change of $\langle 2_1^+ || M1 || 2_2^+ \rangle$ was within the error. Therefore, in this analysis, we adopted the value given in the nuclear data sheets [12].

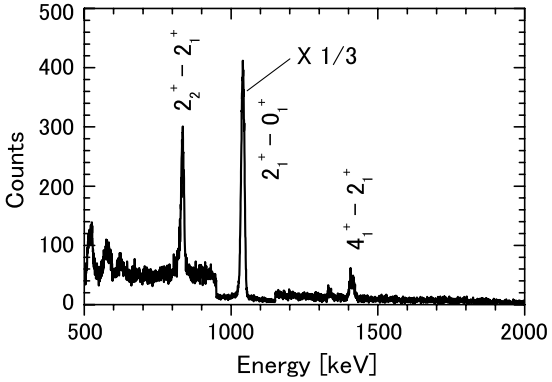

Fig. 1. A γ-ray spectrum obtained after Doppler-shift correction. This spectrum was measured with a Ge detector placed at $\theta = 90°$ and $\phi = 206.6°$.

The data set was analyzed with the least-square search code GOSIA [22], which searches the standard χ^2 minimum changing the matrix elements to reproduce available experimental data. The code takes into account the effects of the deorientation and the electron conversion on the gamma yield. The correction for the finite solid angle of Ge detectors is also done according to the method established by Krane [26]. In the χ^2 minimum search process, the efficiency of each particle detector segment is normalized, using the γ-ray yields of the $2_1^+ \rightarrow 0_1^+$ transition. Once the particle detector efficiencies are found, the matrix elements including the one used for the normalization are derived from the γ-ray yield pattern and the spectroscopic data. This iteration procedure is repeated until it reaches the χ^2 minimum. This makes it possible to analyze the data set without absolute particle detector efficiencies.

It should be noted that the $4_1^+ \rightarrow 0_1^+$ $E4$ transition observed in the ^{66}Zn(p, p$'\gamma$) experiment [27] was omitted in this analysis because it was not confirmed by any other

Table 1. Spectroscopic data: the input data are taken from previous experiments [12]; the results are calculated from the matrix elements given in table 2.

		Inputs	Results
Branching ratio	$I_\gamma(2_2^+ \to 0_1^+)/I_\gamma(2_2^+ \to 2_1^+)$	0.0040 (3)	0.004 (20)
Lifetime [ps]	$\tau(2_1^+)$	2.38 (9)	2.33 (15)
$E2/M1$ mixing ratio	$\delta(2_2^+ \to 2_1^+)$	$-1.9(3)$	$-2.0(7)$

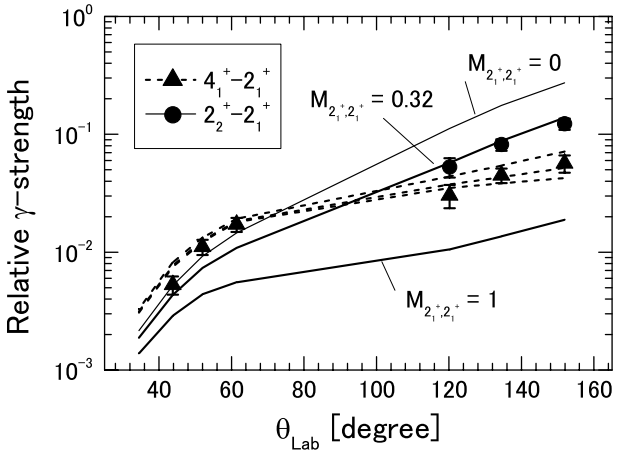

Fig. 2. A comparison between experimental and simulated relative γ strengths for the Ge detector placed at $\theta = 90°$. The horizontal axis is the angle of the center of each particle detector segment in the laboratory frame. The vertical axis is the γ strength divided by the $2_1^+ \to 0_1^+$ γ strength. The circular and triangular symbols indicate experimental values of the relative γ strength of the $2_2^+ \to 2_1^+$ and $4_1^+ \to 2_1^+$ transitions, respectively. The solid and dashed lines are the calculated relative γ strength.

Table 2. Reduced matrix elements $\langle I_i||E2||I_f\rangle$ [eb], $\langle 2_1^+||M1||2_2^+\rangle$ [μ_N], and a diagonal matrix moment $\langle I_i||E2||I_i\rangle$ [eb]. Values without positive or negative sign are absolute values. The signs of matrix elements are given assuming the $\langle 2_1^+||E2||0_1^+\rangle$ is positive. Previously obtained experimental matrix elements are calculated with the $B(E2)$ values given by ref. [12].

	$I_i \to I_f$	Present	Previous [12]
$\langle I_i\|\|E2\|\|I_f\rangle$	$2_1^+ \to 0_1^+$	+0.380 (12)	0.3766 (7)
	$2_2^+ \to 0_1^+$	+0.005 (13)	0.016 (3)
	$2_2^+ \to 2_1^+$	+0.57 (10)	1.69 (3)
	$4_1^+ \to 2_1^+$	+0.500 (10)	0.71 (8)
$\langle I_i\|\|M1\|\|I_f\rangle$	$2_2^+ \to 2_1^+$	-0.20 (6)	0.62 (14)
$\langle I_i\|\|E2\|\|I_i\rangle$	2_1^+	+0.32 (10)	

experiments, and the influence to our experiment will be negligibly small, even if it exists.

Because the observed γ yields of $2_2^+ \to 2_1^+$ transition in coincidence with forward particle detectors were too weak, and because there exist few spectroscopic data that are useful for the analysis, the diagonal matrix elements could not be determined independently. We, therefore, introduced the relation of $Q_{2_2^+} = -Q_{2_1^+}$ and $Q_{4_1^+} = 1.266 Q_{2_1^+}$ based on the simple rotation-vibration model, assuming that the intrinsic moments of the states are the same. As has been pointed out in refs. [1–3,28,29], the low-lying states of $^{62-66}$Zn isotopes can be interpreted as collective band structures. Therefore, it would be reasonable to consider the intrinsic moments of the states would have the same value, while the 2_2^+ can be considered as a kind of γ band head with $K = 2$. Introducing the assumption mentioned above, however, does not mean the denial of the pure vibrational structure of this nucleus, because the χ^2 minimum of the GOSIA analysis is supposed to appear around $Q_{2_1^+} = 0$, if the nucleus is pure vibrational.

Figure 2 shows a plot of experimental and calculated normalized γ-yields for one of the Ge detectors, which was located at $\theta = 90°$ and $\phi = 206.6°$. The horizontal axis of this figure is the angle of the center of each particle detector segment in the laboratory frame. The circular and triangular points indicate experimental relative γ yields of the $4_1^+ \to 2_1^+$ transition and those of the $2_2^+ \to 2_1^+$ transition, respectively. The solid and dashed lines in fig. 2 connect calculated values for the $2_2^+ \to 2_1^+$ and $4_1^+ \to 2_1^+$ transitions, respectively. Those calculations were carried out with one of the functions of the GOSIA program, demonstrating how the $M_{2_1^+,2_1^+}$ matrix elements have an influence on the yield pattern. (The value M_{ij} is an $E2$ matrix element defined by $\langle i||E2||j\rangle$.) The $M_{2_2^+,2_2^+}$ and $M_{4_1^+,4_1^+}$ matrix elements were changed so as to be proportional to the $M_{2_1^+,2_1^+}$, while the other matrix elements were fixed to the values of the result of this analysis given in table 2. It can be easily seen in fig. 2 that the yield ratios of $2_2^+ \to 2_1^+$ transition are sensitive to the $M_{2_1^+,2_1^+}$ matrix element, while those of the $4_1^+ \to 2_1^+$ transition are insensitive. As the result of this analysis, we obtained that $M_{2_1^+,2_1^+} = +0.32 \pm 0.10$ eb.

It should be noted that we also analyzed the experimental data with the assumption that the intrinsic quadrupole moments of the 2_1^+, and 4_1^+ states are the same, and that of the 2_2^+ state is independent of that of the 2_1^+ state. The result of GOSIA analysis shows no major differences; all matrix elements agree within the errors.

It is often pointed out that the sign of the interference term, P_3 $(= M_{0_1^+,2_1^+} M_{2_1^+,2_2^+} M_{2_2^+,0_1^+})$, influences the sign and magnitude of the quadrupole moment. In this case, the influence of the P_3 is too little to change the quadrupole moment drastically. It is due to the small value

Table 3. Comparison of experimental and theoretical $B(E2)$ [e^{2}fm^4] and $Q(2_1^+)$ [efm^2]. (NDS: Nuclear Data Sheets [12]. DCM: Deformed Configuration Mixing shell model [28]. SM: Shell Model [5]. PHFB: Projected Hartree-Fock-Bogoliubov method [30].)

	Experimental		Theoretical calculation		
	present	NDS	DCM	SM	PHFB
$B(E2; 2_1^+ \to 0_1^+)$	288 (18)	284 (11)	203	270 (4)	291
$B(E2; 2_2^+ \to 0_1^+)$	0.06 (28)	0.05 (2)	0.2	0.5 (10)	
$B(E2; 2_2^+ \to 2_1^+)$	650 (228)	5700 (220)	95	260 (40)	
$B(E2; 4_1^+ \to 2_1^+)$	278 (11)	560 (130)	184	330 (50)	
$Q(2_1^+)$	+24 (8)		−16	−19	+34.3

Table 4. Experimentally obtained lifetimes in ps. The present values are deduced from the matrix elements given in table 2.

Level	Present	^{63}Cu(α, 2nγ)[a]	^{64}Ni(α, pγ)[b]	^{63}Cu(α, 2nγ)[c]	(n, n$'\gamma$)[d]	Coulomb [e]	^{66}Zn(e, e$'$)[f]
2_1^+	2.33 (15)	1.8 $(^{+12}_{-8})$	2.5 $(^{+5}_{-2})$			2.25 (14)	2.39 (14)
2_2^+	2.5 (7)	1.0 $(^{+8}_{-2})$	1.2 $(^{+5}_{-3})$	0.27 (10)	1.1 $(^{+6}_{-3})$		
4_1^+	0.52 (2)	0.4 $(^{+2}_{-1})$	1.2 $(^{+5}_{-4})$	0.21 (11)	0.24 $(^{+7}_{-4})$		

([a]) From ref. [13].
([b]) From ref. [14].
([c]) From ref. [15].
([d]) From ref. [16].
([e,f]) Those values are deduced from the $B(E2)$'s in refs. [31] and [32], respectively.

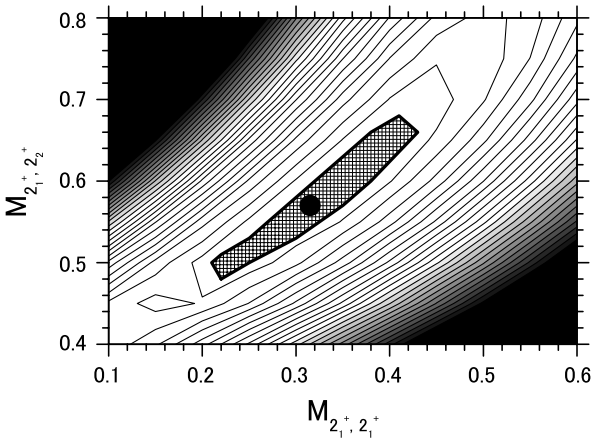

Fig. 3. A contour map of χ^2 in the $(M_{2_1^+,2_1^+}, M_{2_1^+,0_1^+})$ space. The other matrix elements except for the $M_{2_2^+,2_2^+}$ and $M_{4_1^+,4_1^+}$ are fixed to the values given in table 2. The $M_{2_2^+,2_2^+}$ and $M_{4_1^+,4_1^+}$ are changed so as to be proportional to the $M_{2_1^+,2_1^+}$. The black dot displays the χ^2 minimum. The hatched area indicates the confidence limit within 1σ.

of the $M_{2_2^+,0_1^+}$. The error of the $M_{2_2^+,0_1^+}$ is larger than the center value as seen in table 2.

The results of the GOSIA analysis are given in table 2. Totally four $E2$ and a $M1$ matrix elements are determined, as well as one diagonal matrix element. The sign of matrix elements are given assuming the $\langle 2_1^+||E2||0_1^+\rangle$ is positive. The errors of the matrix elements were determined from the χ^2 distribution in the vicinity of the minimum. Cross-correlation effects are also included. The errors are given by the range where the total probability of a parameter set is at the confidence limit of 68.3% [22]. The errors of the $M_{2_1^+,2_1^+}$ and $M_{2_1^+,2_2^+}$ matrix elements are comparably large because there exists a strong correlation between the matrix elements in the χ^2 distribution. Figure 3 displays a contour map of χ^2 in the space of these two matrix elements. The other matrix elements are fixed except for the $M_{2_2^+,2_2^+}$ and $M_{4_1^+,4_1^+}$, which were synchronized with the $M_{2_1^+,2_1^+}$. The black dot displays the χ^2 minimum. A long χ^2 valley exists as seen in fig. 3. The confidence limit is indicated with the hatched area. As seen in table 1, the result reproduced the spectroscopic data quite well.

4 Discussion

The $B(E2)$ values deduced from the present experiment are given in table 3. The $B(E2; 2_1^+ \to 0_1^+)$ agrees with the adopted $B(E2)$ value of NDS [12]; but the $B(E2; 4_1^+ \to 2_1^+)$ is about half of the adopted value, and the $B(E2; 2_2^+ \to 2_1^+)$ is about one-ninth. Those adopted values were mainly based on the lifetime measurements, which are listed in table 4. The present 2_1^+ lifetime agrees well with the previous experimental values. For the 4_1^+ state, the present lifetime agrees with that of the ^{63}Cu$(\alpha, 2n\gamma)$ experiment [13] within the error, but does not agree with the other three experiments. For the 2_2^+ state, the present lifetime is longer than the others. This means that the present experimental $B(E2; 2_2^+ \to 2_1^+)$ is smaller than those deduced from the lifetime experiments. The 2_1^+ quadrupole moment was determined

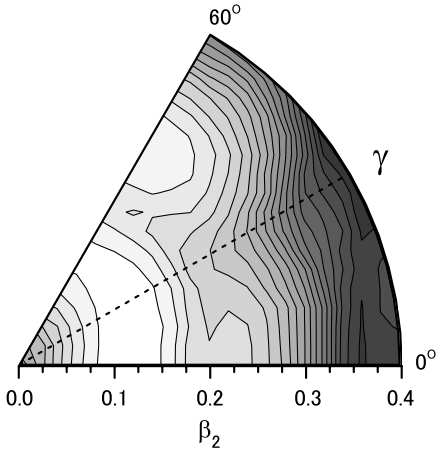

Fig. 4. A potential energy surface of ^{66}Zn calculated with the cranked Nilsson-Strutinsky model. The energy difference between the contour lines is 250 keV. The dashed line indicates $\gamma = 30°$.

experimentally for the first time. The value suggests that the ground band of ^{66}Zn is slightly oblate deformed.

Because the $B(E2; I+2 \rightarrow I)$'s between the 0_1^+, 2_1^+, and 4_1^+ states are enhanced as high as about $280\,\mathrm{e^2fm^4}$, and the $B(E2; 6_1^+ \rightarrow 4_1^+)$ is also enhanced as $238 \pm 95\,\mathrm{e^2fm^4}$ [12], one can consider them as quasirotational band. (Note that the assignment for the 4182.7 keV state is not established [12], but we dealt with it as $J^\pi = 6^+$, as other articles did [5,33]. The original assignment of 6^+ has been made by Bruandet *et al.* [29].) Similar band structure was observed and pointed out for the ^{64}Zn and ^{62}Zn [1–3].

The deformed configuration mixing shell model (DCM) calculation [28] explains well the ground band structure. In this calculation $2p_{3/2}1f_{5/2}2p_{1/2}1g_{9/2}$ model space with ^{56}Ni core was used. The ground band which ends at the 8^+ is predominated by the $(2p_{3/2}1f_{5/2}2p_{1/2})^{10}$ configuration. The ratios of the present experimental $B(E2)$ values were reproduced well, while their magnitudes were underestimated. The shell model (SM) calculation was carried out in the $(2p_{3/2}1f_{5/2}2p_{1/2})$ model space with ^{56}Ni core [5]. This also shows good agreement with the $B(E2)$ values in the ground band. Those calculations suggest that the influence of the $1g_{9/2}$ orbit on the ground band is very weak. While those theoretical calculation reproduce the ground band $B(E2)$ values rather well, they do not reproduce the experimental 2_1^+ quadrupole moment; they predicted prolate deformation for the 2_1^+ state. Only the calculation with the projected Hartree-Fock-Bogoliubov (PHFB) method [30], which was carried out for the attempt of reproducing the inelastic electron scattering form factors for the $0^+ \rightarrow 2^+$ and the $2^+ \rightarrow 4^+$ transitions, predicted the oblate deformation.

For the interpretation of the experimental data one can also use the triaxial rotor model [34]. From the experimental quadrupole moment $Q_{2_1^+}$ and the $B(E2; 2_1^+ \rightarrow 0_1^+)$, the triaxiality can be deduced to be $\gamma = 36°^{+8}_{-3}$, which clearly deviates from $\gamma = 60°$ (oblate shape). Figure 4 shows a potential energy surface calculated with the cranked Nilsson-Strutinsky model [35]. It shows a γ-unstable character at the potential minimum. It seems that such a model with a soft triaxial potential explains the structure of ^{66}Zn.

5 Summary

Multiple Coulomb excitation experiment with a ^{66}Zn projectile bombarding $^{\mathrm{nat}}$Pb target was carried out at the tandem and booster accelerator facility of Tokai/JAERI. The obtained data was analyzed with the least-square search code GOSIA. The quadrupole moment of the 2_1^+ state and four $B(E2)$ values were obtained, in which the $B(E2)$'s of the $2_2^+ \rightarrow 2_1^+$ and $4_1^+ \rightarrow 2_1^+$ transitions were revised. According to the $B(E2)$ values, the ground band can be interpreted as a quasirotational band. The DCM and SM calculations suggest that the ground band is probably predominated by the $2p_{3/2}$, $1f_{5/2}$, and $2p_{1/2}$ orbits. The 2_1^+ state was found to have a positive quadrupole moment, which supported the calculation carried out with the PHFB method to reproduce the inelastic electron scattering form factors, while other theoretical calculations predicted it was prolate. The rigid triaxial rotor model suggests that this nucleus has a gamma around 30°, and the cranked Nilsson-Strutinsky model suggests that this value is an average over the large fluctuation. It seems that such a model with a soft triaxial potential may explain the matrix elements and the energy levels of ^{66}Zn.

The authors are grateful to the JAERI tandem and booster accelerator facility for their support and assistance for this study with a ^{66}Zn ion beam.

References

1. L. Mulligan, R.W. Zurmühle, D.P. Balamuth, Phys. Rev. C **19**, 1295 (1979).
2. N.J. Ward, L.P. Ekström, G.D. Jonse, F. Kearns, T.P. Morrison, O.M. Mustaffa, D.N. Simister, P.J. Twin, R. Wadsworth, J. Phys. G **7**, 815 (1981).
3. D.N. Simister, G.D. Jones, F. Kearns, A. Kogan, P.R.G. Lornie, T.P. Morrison, O.M. Mustaffa, H.G. Price, P.J. Twin, R. Wadsworth, J. Phys. G **4**, 1127 (1978).
4. B. Crowell, P.J. Ennis, C.J. Lister, W.R. Schief jr., Phys. Rev. C **50**, 1321 (1994).
5. J.F.A. Van Hienen, W. Chung, B.H. Wildenthal, Nucl. Phys. A **269**, 159 (1976).
6. Y. Toh, T. Czosnyka, M. Oshima, T. Hayakawa, H. Kusakari, M. Sugawara, Y. Hatsukawa, J. Katakura, N. Shinohara, M. Matsuda, J. Phys. G **27**, 1475 (2001).
7. Y. Toh, T. Czosnyka, M. Oshima, T. Hayakawa, H. Kusakari, M. Sugawara, Y. Hatsukawa, J. Katakura, N. Shinohara, M. Matsuda, Eur. Phys. J. A **9**, 353 (2000).
8. B. Kotlinski, T. Czosnyka, D. Cline, J. Srebrny, C.Y. Wu, A. Backlin, L. Hasselgren, L. Westerberg, C. Baktash, S.G. Steadman, Nucl. Phys. A **519**, 646 (1990).
9. A.E. Kavka, C. Fahlander, A. Bäcklin, D. Cline, T. Czosnyka, R.M. Diamond, D. Disdier, W.J. Kernan, L. Kraus, I. Linck, N. Schulz, J. Srebrny, F.S. Stephens, L.E. Svensson, B. Varnestig, E.G. Vogt, C.Y. Wu, Nucl. Phys. A **593**, 177 (1995).

10. W. Andrejtscheff, P. Petkov, Phys. Lett. B **329**, 1 (1994).
11. W. Andrejtscheff, P. Petkov, Phys. Rev. C **48**, 2531 (1993).
12. M.R. Bhat, Nuclear Data Sheets **83**, 789 (1998).
13. U.Yu. Zhovliev *et al.*, Izv. Akad. Nauk. SSSR, Ser. Fiz. **45**, 1879 (1981).
14. C. Morand *et al.*, J. Phys. (Paris) **11**, 1319 (1977).
15. M. Ivascu *et al.*, Nucl. Phys. A **218**, 104 (1974).
16. Y.G. Kosyak, D.K. Kaipov, L.V. Chekushina, Bull. Acad. Sci. USSR, Phys. Ser. **49**, 55 (1985). (Translation of Izv. Akad. Nauk SSSR. Ser. Fiz., **49**, 895 (1985).)
17. K. Alder, A. Winther, *Coulomb Excitation* (Academic, New York, 1966).
18. K. Alder, A. Winther, *Electromagnetic Excitation - Theory of Coulomb Excitation with Heavy Ions* (North-Holland Publishing Co., 1975).
19. D. Cline, Ann. Rev. Nucl. Part. Sci. **36**, 683 (1986).
20. K. Furuno, M. Oshima, T. Komatsubara, K. Furutaka, T. Hayakawa, M. Kidera, Y. Hatsukawa, M. Matsuda, S. Mitarai, T. Shizuma, T. Saitoh, N. Hashimoto, H. Kusakari, M. Sugawara, T. Morikawa, Nucl. Instrum. Methods Phys. Res. A **421**, 211 (1999).
21. Y. Toh, M. Oshima, T. Hayakawa, Y. Hatsukawa, J. Katakura, M. Matsuda, H. Iimura, H. Kusakari, D. Nishimiya, M. Sugawara, Y.H. Zhang, Rev. Sci. Instrum. **73**, 47 (2002).
22. T. Czosnyka, D. Cline, L. Hasselgren, C.Y. Wu, Nucl. Phys. A **458**, 123 (1986).
23. T. Czosnyka, C.Y. Wu, D. Cline, Bull. Am Phy. Soc. **28**, 745 (1983).
24. T. Hayashi *et al.*, J. Phys. Soc. Jpn. **27**, 1375 (1969).
25. A. Schwarzschild, L. Grodzins, Phys. Rev. **119**, 276 (1960).
26. S.K. Krane, Nucl. Instrum. Methods **98**, 205 (1972).
27. A.E. Wntropov, D.R. Gandarias, V.P. Gusev, P.P. Zarubin, P.D. Ioannu, Izv. Akad. Nauk. SSSR, Ser. Fiz. **39**, 2139 (1975); Bull. Acad. Sci. USSR, Phys. Ser. **39**, 112 (1975).
28. D.P. Ahalpara, K.H. Bhatt, S.P. Pandya, Nucl. Phys. A **371**, 210 (1981).
29. J.F. Bruandet, M. Agard, A. Giorni, J.P. Longequeue, C. Morand, Tsan Ung Chan, Phys. Rev. C **12**, 1739 (1975).
30. P.K. Raina, Phys. Rev. C **37**, 1427 (1988).
31. P.H. Stelson, F.K. McGowan, Nucl. Phys. **32**, 652 (1962).
32. R. Neuhausen, J.W. Lightbody jr., S.P. Fivozinsky, S. Penner, Nucl. Phys. A **263**, 249 (1976).
33. S.K. Sharma, Phys. Rev. C **22**, 2612 (1980).
34. A.S. Davydov, G.F. Filipov, Nucl. Phys. **8**, 237 (1958).
35. T. Bengtsson, I. Ragnarsson, S. Åberg, in *Computational Nuclear Physics 1*, edited by K. Langanke, J.A. Maruhn, S.E. Koonin (Springer-Verlag, Berlin, 1991) p. 51.